Electronic Supplementary Material (ESI) for Polymer Chemistry.

Supporting Information for:

Tuning PNIPAm Self-Assembly and Thermoresponse: Roles of Hydrophobic End-Groups and Hydrophilic Comonomer

Monica L. Ohnsorg,[†] Jeffery M. Ting,[‡,⊥] Seamus D. Jones,[‡,⊥] Seyoung Jung,[‡] Frank S. Bates,[,‡] and Theresa M. Reineke[*,†]*

[†]Department of Chemistry, [‡]Departments of Chemical Engineering and Materials Science, University of Minnesota, Minneapolis, MN 55455

Present Addresses: [⊥] J.M.T.: Institute for Molecular Engineering, University of Chicago, Chicago, Illinois 60637, United States; S.D.J.: Departments of Chemical Engineering and Materials, University of California, Santa Barbara, California 93117, United States.

*Corresponding Email: bates001@umn.edu, treineke@umn.edu

Table of Contents:

1 Materials and Methods

1.1 Materials and Synthesis Procedure

The following reagents were used as received from Aldrich, unless otherwise noted: N-isopropylacrylamide (NIPAm, >99%), N,N-dimethylacrylamide (DMA, 99+%), 2-(dodecylthiocarbonothioylthio)propionic acid (DoPAT, 97%), 3,5-Bis(2-dodecylthiocarbonothioylthio-1-oxopropoxy)benzoic acid (BDOBA, 98%), 2,2′-azobis(2-methylpropionitrile) (AIBN, 98%), 1,4-dioxane (Fisher Chemical, ≥99%), hexane (Fisher Chemical, ≥98.5%), diethyl ether (Fisher Chemical, anhydrous, ≥99%), tetrahydrofuran (THF, Fisher Chemical, ≥99.9%), N,N-dimethylformamide (DMF, ≥99.9%), methyl acrylate (MA, 99%), n-propylamine (≥99%), tris(2-carboxyethyl)phosphine hydrochloride (TCEP, ≥98%), trimethylsilyl propanoic acid (TSP, 98 atom % D), deuterium oxide (D_2O, 99.9 atom % D), and chloroform-*d* (99.8 atom % D). DMA and MA were passed through activated basic alumina to remove trace inhibitors.

For each reversible addition-fragmentation chain transfer (RAFT) polymerization, the initial CTA to initiator ratio ($[CTA]_0$ / $[I]_0$) was kept at 10 to 1, and the initial monomer concentration was fixed at 1 M in 1,4-dioxane. In a representative example for the synthesis of PNIPAm in $N_{52}D_{25}N_{30}$-C12, NIPAm (6.79, 60 mmol), DoPAT (0.438 g, 1.25 mmol), and AIBN (0.0205 g, 0.125 mmol) were dissolved in 1,4-dioxane (60 mL) in a dried round bottom flask. The yellow-colored solution was sealed and degassed with inert nitrogen at room temperature for ~ 30 min. An initial sample was taken to monitor monomer conversion. The reaction vessel was then submerged into a preheated, stirred oil bath maintained at 70 °C overnight. The disappearance of the monomer vinyl proton peaks (^{1}H NMR, $CDCl_3$: δ 5.8 (m, 1H, =C-**H**); 6.1 (m, 1H, =C-**H**); 6.4 (m, 1H, =C-**H**) ppm) was used as a reference to quench by cooling to 0 °C and opening the flask

to air. The crude product was precipitated into a hexane/diethyl ether (60/40, *v*/*v*, %) mixture to remove residual monomer and solvent. Minimal THF was used to dissolve the solid, followed by a repeated precipitation with the hexane/diethyl ether mixture. The precipitated sample was filtered and dried under vacuum overnight. For chain extension, the theoretical molecular weight of each block was used for the RAFT macro-CTA. In a representative example for the synthesis of PNIPAm-PDMA in $N_{52}D_{25}N_{30}$-C12, DMA (1.88 g, 19 mmol), PNIPAm macro-CTA (2.64 g, 0.463 mmol), and AIBN (0.00761 g, 0.0463 mmol) were dissolved in 1,4-dioxane (19 mL) in a round bottom flask; the same protocol described above was followed thereafter.

Theoretical Number of Living Chains Calculation:

Polymerizations were conducted for t = 18 h with 2,2'-azobis(2-methylpropionitrile) (AIBN), and the initial CTA to initiator ratio ($[CTA]_0$ / $[I]_0$) was maintained at 10:1 for all reactions. We calculated the theoretical number fraction of living chains (L)[1] to be ~97% under these conditions using Equation S-1,

$$L = \frac{[\mathrm{CTA}]_0}{[\mathrm{CTA}]_0 + 2f[\mathrm{I}]_0\left(1-e^{-k_d t}\right)\left((1-f_c)/2\right)} \quad \text{(S-1)}$$

which was deemed sufficiently high for multiblock preparation. This L value provides a metric of livingness in the reversible deactivation radical polymerization mechanism. In other words, this describes the number fraction of chains that retain the desired ω-end group thiocarbonylthio moiety for chain extension. In this calculation, we used the initiator decomposition rate constant for AIBN in 1,4-dioxane at 65 °C ($k_d = 1.9254 \times 10^{-5}$ s^{-1}), reported by Gody *et al.*,[2] and assumed no side reactions, a conservative initiator efficiency (f) of 0.5, and 100% radical termination by disproportionation ($f_c = 0$).

1.2 Polymer Characterization

Size-Exclusion Chromatography with Multi-Angle Light Scattering (SEC-MALS). SEC-MALS with ASTRA® 6 software was used to determine the absolute molecular weight (M_n) and dispersity ($Đ$) of prepared multiblock polymers. The d*n*/dc values of poly(NIPAm) and poly(DMA) were determined using an Abbe Refractometer with a red LED light source, varying polymer concentrations (0-40 mg/mL) in SEC-grade THF at 25 °C.

Approximately 2-4 mg of sample was dissolved in 1 mL THF and filtered through a 0.2 μm membrane filter, and the solution was introduced to the instrument with a THF mobile phase at a flow rate of 1.0 mL/min at 25 °C. The run time for the method was 45 min. SEC-MALS experiments were conducted on an Agilent 1260 Infinity high performance liquid chromatography system with one Waters Styragel guard column and three Waters Styragel columns (HR6, HR4, and HR1) with pore sizes suitable for materials with effective molecular weights from 100 to 10,000,000 g/mol. The instrument was equipped with an Agilent 1260 Infinity Variable Wavelength Detector set at a monitoring wavelength of 254 nm (80 Hz data collection frequency), a Wyatt Optilab T-rEX refractive index detector operated at a wavelength of 658 nm, and a Wyatt Dawn Heleos II multiangle light scattering (MALS) detector operated at a laser wavelength of 663.6 nm (18 angles from 10° to 160°).

The statistical copolymers were analyzed on a SEC-MALS instrument in DMF containing 0.05 M LiBr because of repairs and column changes in the THF instrument. Approximately 2-4 mg of sample was dissolved in 1 mL of the mobile phase and filtered through a 0.2 μm membrane filter before introduction into an Agilent Infinity 1200 HPLC system operating at 50 °C and 1.0 mL/min. The instrument was equipped with two Viscotek I-MBMMW3078 columns, a Wyatt Optilab T-rEX differential refractive index detector, and a Wyatt HELEOS-II MALS detector.

dn/dc Calculations. The experimentally-measured DP was calculated using ^{1}H NMR spectroscopy assuming one RAFT agent per chain. We measured the d*n*/dc of RAFT-mediated PNIPAm and PDMA in tetrahydrofuran (THF) at 23 °C to be 0.1310 and 0.2146 mL/g, respectively. The change in refractive index value for each multiblock $(dn/dc)_{block}$ was calculated using Equation S-2, which assumes that the $(dn/dc)_{block}$ is a weighted linear combination of the change in the constitutive monomers' refractive index values:

$$\left(\frac{dn}{dc}\right)_{block} = w_A\left(\frac{dn}{dc}\right)_A + (1-w_A)\left(\frac{dn}{dc}\right)_B . \quad \text{(S-2)}$$

Here, w_A is the weight fraction of monomer A, and $(dn/dc)_{A/B}$ represents the refractive index of monomer A/B.

Proton Nuclear Magnetic Resonance (^{1}H NMR) Spectroscopy. ^{1}H NMR spectroscopy experiments were performed using a Bruker Avance III HD 500 spectrometer equipped with a 5 mm Prodigy TCI cryoprobe with z-axis gradients at 22 °C using a 10 second relaxation delay and at least 16 transients without spinning to reduce signal-to-noise ratio in $CDCl_3$. ^{1}H NMR data was processed with iNMR (http://www.inmr.net) and Bruker TopSpin 3.5 pl 7.

1.3 Solution Characterization

Solution Preparation. Solutions were prepared by diluting a 25 mg/mL stock solution of dried polymer in PBS buffer (pH = 6.5) prepared the night before to allow the dried polymer to fully dissolve. For light scattering measurements, the diluted sample was measured immediately. For cloud point measurements, the stock solution was diluted to 1 mg/mL in an ampule, sealed, and measured over the course of 7 days.

Cloud Point Experiments. Polymer solutions (1 mg/mL) were transferred to sealed glass ampules to minimize evaporation for cloud point measurements. The samples were placed in the

stage and heated from room temperature to 50 °C or 60 °C at an effective heating rate of 0.25 °C/min. The samples were cooled to room temperature using a fan. The optical transmittance of the solutions from a 30 mW 633 nm HeNe laser source was recorded from the reading on a photometer (Spex Industries Laser Power Meter 1448, Metuchen, NJ). The measured transmittance as a function of temperature was normalized to the constant transmittance values near room temperature, and the cloud point was defined when the solution decreased to less than 80% of the fully dissolved solution.

DOSY 2D NMR Spectroscopy Experiments. All NMR measurements were performed on a Bruker Advance III 500 MHz spectrometer in a D_2O-based PBS buffer solution (pH 6.5) with added standard, trimethylsilylpropanoic acid (TSP). DOSY 2D NMR experiments were collected using the 'ledbpgp2s' pulse program from Bruker Topspin software. Diffusion data was acquired at 27 °C and 50 °C for each multiblock polymer over a gradient pulse amplitude ranging from 2 to 95% over 25 scans. Temperature settings were calibrated using ethylene glycol by measuring the shift difference between the two proton NMR signals, which depend strongly on temperature. Bruker Topspin software was used to calculate the diffusion constant from the 2D DOSY spectra and to process the DOSY maps with diffusion plotted on a logarithmic scale from -9 diffusion maximum to -12 diffusion minimum.

Dynamic Light Scattering (DLS) Experiments. DLS samples were passed through 0.20 μm syringe filters before transfer into dust-free 0.25 in. diameter glass tubes. DLS measurements were performed on an in-house photometer (30 mW laser power, avalanche photodiode detector with a 200 μm pinhole) over a range of angles (60-120°) with a Brookhaven BI- 200SM goniometer and a Brookhaven BI-9000AT correlator at λ = 637 nm and temperatures of 23 or 50 °C to measure the hydrodynamic radius R_h. A dust-free decalin bath was used to match the refractive index of

glass. The size distribution was also assessed through the REPES Laplace inversion routine.[3] The dispersity of particle size was quantified by the reduced second cumulant μ_2/Γ^2 with Γ being the mean decay rate of first-order scatting autocorrelation.

Static Light Scattering (SLS) Experiments. SLS samples (1 mg/mL) were prepared and conducted using the same instrument described in the DLS protocol above. The partial Zimm analysis enables the determination of the weight-average molecular weight from measurements of the Rayleigh ratio (R_θ) at various wavevectors from $\theta = 50°$ to 150°. The measurements were conducted at 25 °C and 50 °C. The data was extrapolated to the y-axis and the intercept was used to calculate the weight average molecular weight of the aggregate in solution. By approximating the number of polymer chains per aggregate, solution structures were hypothesized from the hydrodynamic radius and aggregation behavior.

2 Experimental: Polymer Synthesis, Characterization, and Post-Synthetic Modification

2.1 Statistical Copolymer Synthesis Characterization

Poly(NIPAm-*co*-DMA) was synthesized according to previous work,[4] using both DoPAT and BDOBA RAFT CTAs. Fig. S1 shows the representative characterization of poly(NIPAm-*co*-DMA)$_{107}$-C12 and C12-poly(NIPAm-*co*-DMA)$_{129}$-C12 with ^{1}H NMR spectroscopy and SEC-MALS with mobile phase of DMF + 0.05M LiBr. The d*n*/dc values of PNIPAm[5] and PDMA[6] homopolymers in DMF were taken from the literature (0.0710 and 0.0870 mL/g, respectively) and used to calculate the expected d*n*/dc at the relevant weight fractions.

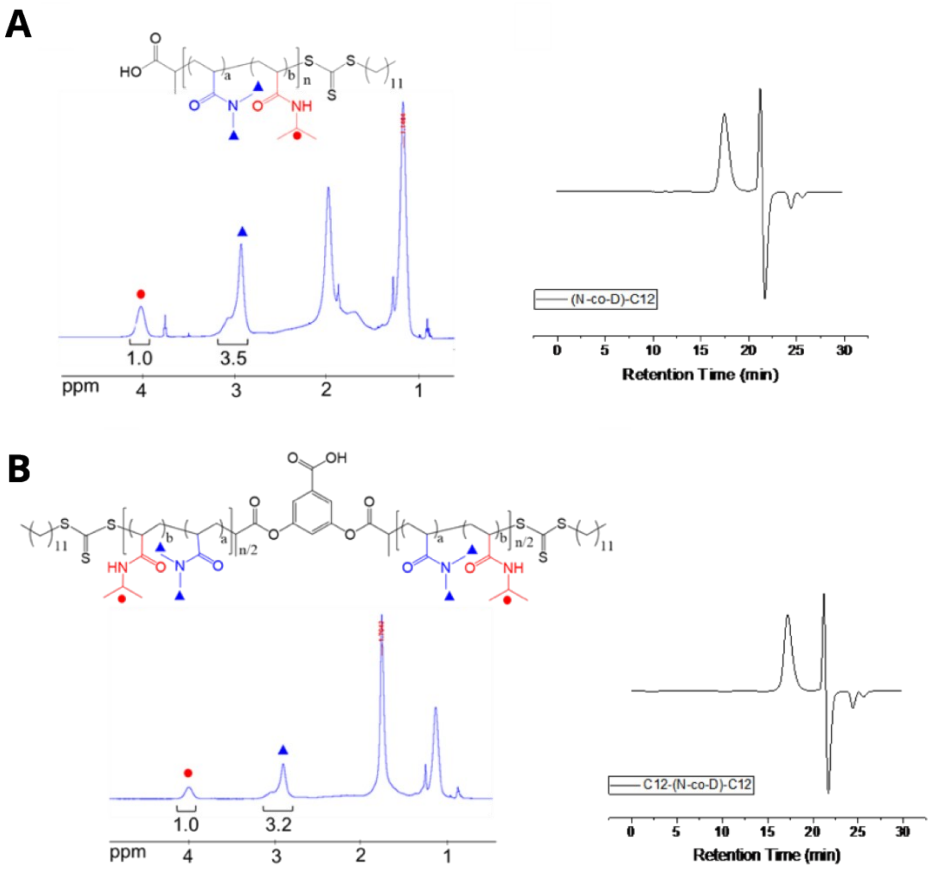

Figure S1. Characterization of (A) poly(NIPAm-*co*-DMA)$_{107}$-C12 and (B) C12-poly(NIPAm-*co*-DMA)$_{129}$-C12 with ^{1}H NMR spectroscopy in $CDCl_3$ (right) and SEC-MALS (left). By ^{1}H NMR spectroscopy, integration of the marked NIPAm and DMA protons results in a calculated 63% and 66% NIPAm chemical composition, respectively. By SEC-MALS in DMF + 0.05 M LiBr, a monomodal RI peak corresponds to M_n = 11,600 and 14,000 g/mol and $Đ$ = 1.03 and 1.06, respectively; the respective d*n*/dc used for the samples in DMF was 0.0769 and 0.0764 mL/g.[5,6]

2.2 ^{1}H NMR Multiblock Copolymer Chemical Composition Calculations

For all NIPAm/DMA systems, the chemical composition was calculated by ^{1}H NMR using the proton peaks of –N-CH– at 4.0 ppm for NIPAm (1 H) and –N-$(CH_3)_2$ at 2.8-3.3 ppm for DMA (6 H). Figs. S2 through S5 show representative ^{1}H NMR spectra for each block polymer extension across all investigated multiblock systems. Equation S-3 shows a sample calculation for the NIPAm composition of the final triblock:

$$\%\ \text{NIPAm} = \frac{(1.00/1)}{(1.00/1)+(3.30/6)} \times 100 = 65\% \qquad \text{(S-1)}$$

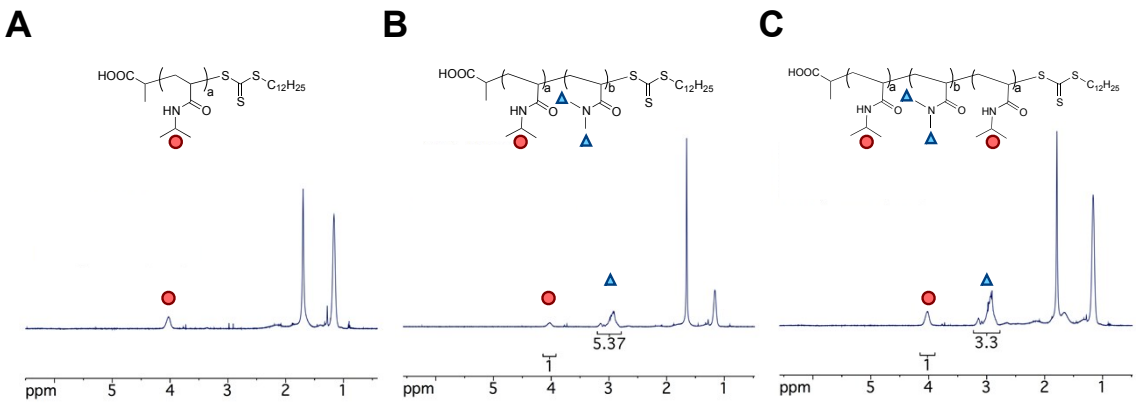

Figure S2. Representative progression of ^{1}H NMR spectra for $N_{52}D_{50}N_{41}$-C12 in $CDCl_3$. The spectra show the purified polymers (A) PNIPAm, (B) PNIPAm-PDMA, and (C) PNIPAm-PDMA-PNIPAm.

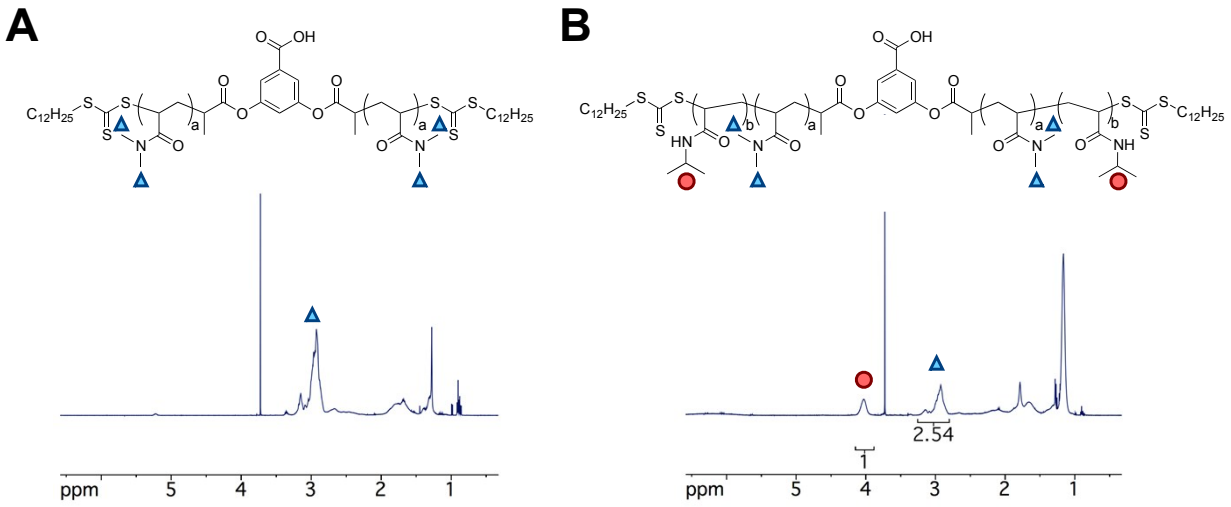

Figure S3. Representative progression of ^{1}H NMR spectra for C12-$N_{69}D_{60}N_{69}$-C12 in $CDCl_3$. The spectra show the purified polymers (A) PDMA and (B) PNIPAm-PDMA-PNIPAm.

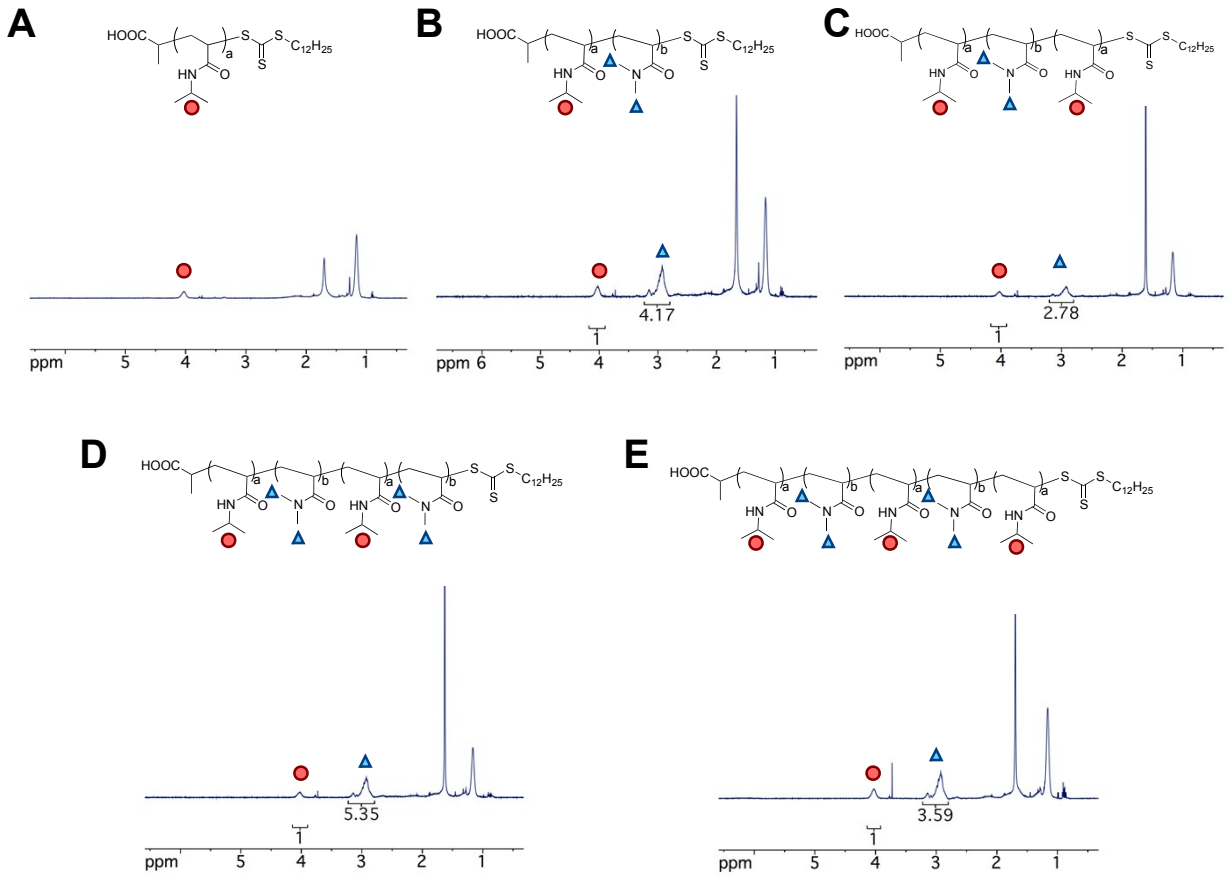

Figure S4. Representative progression of ^{1}H NMR spectra for $N_{35}D_{40}N_{42}D_{23}N_{22}$-C12 in $CDCl_3$. The spectra show the purified polymers (A) PNIPAm, (B) PNIPAm-PDMA, (C) PNIPAm-PDMA-PNIPAm, (D) PNIPAm-PDMA-PNIPAm-PDMA, and (E) PNIPAm-PDMA-PNIPAm-PDMA-PNIPAm.

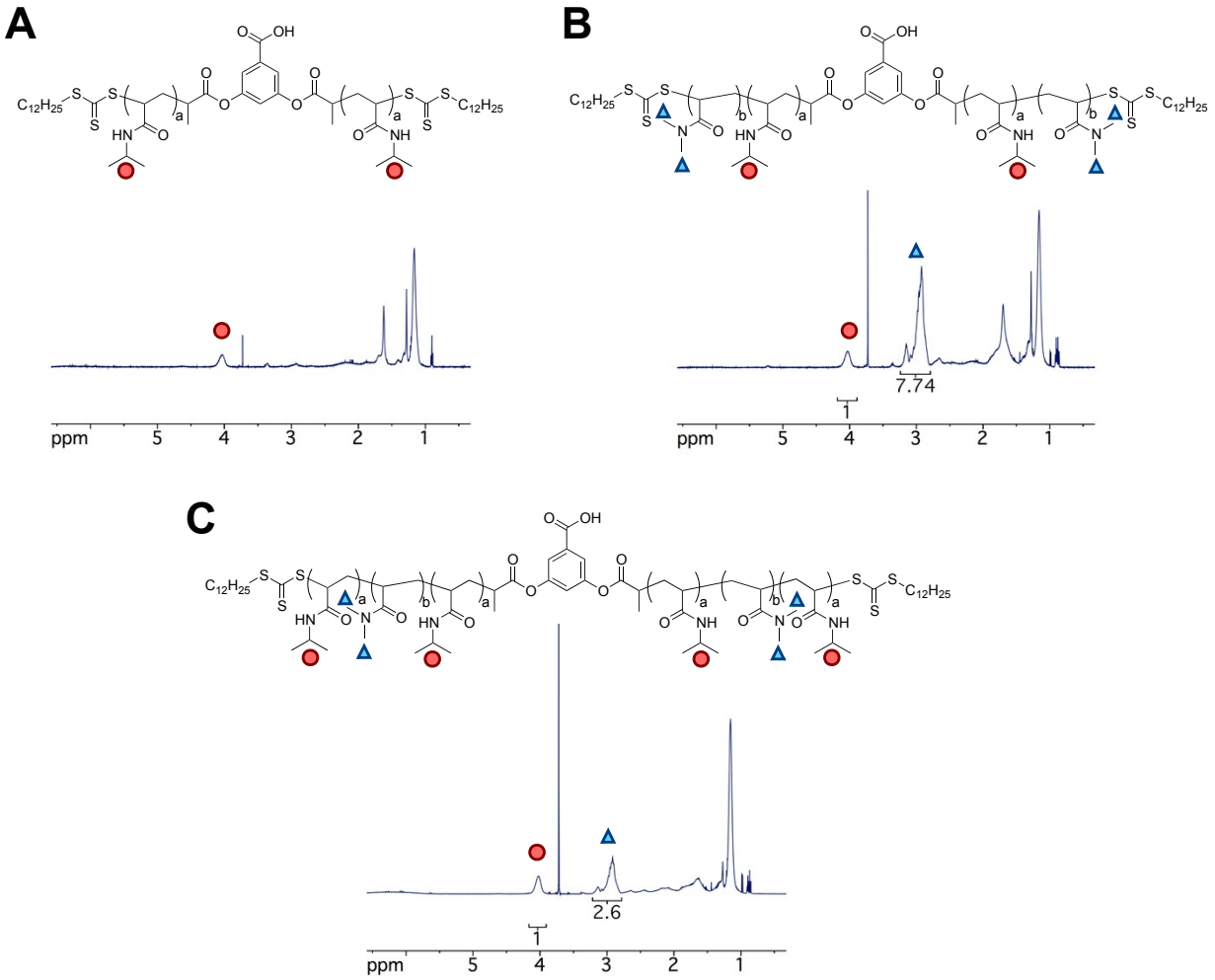

Figure S5. Representative progression of ^{1}H NMR spectra for C12-$N_{46}D_{29}N_{46}D_{29}N_{46}$-C12 in $CDCl_3$. The spectra show the purified polymers (A) PNIPAm, (B) PDMA-PNIPAm-PDMA, and (C) PNIPAm-PDMA-PNIPAm-PDMA-PNIPAm.

The degree of polymerization (DP) of multiblock system was calculated as follows. Equation S3 shows a sample calculation of determining $N_{52}D_{50}N_{41}$-C12:

$$\begin{aligned} DP_{block1} &= (6230 - 351\ \text{g/mol}) / (1 \times 113\ \text{g/mol}) = 52 \\ DP_{block2} &= (49/51) \times 52 = 50 \\ DP_{block3} &= (65/35) \times 50 - 52 = 41 \end{aligned} \quad \text{(S3)}$$

2.3 Detailed Block Extension Synthesis/Characterization

The following contains a detailed summary of the block extension reactions. Table S1 shows the calculated change in refractive index (d*n*/dc) of each block polymer in THF and DMF. Figs. S6 and S7 graphically depict the evolution of the molecular weight and dispersity with increasing blocks in the THF systems.

Table S1. Summary of d*n*/dc calculation for each block extension across all systems.

System[a]	Block Extension No.	Mol Fr NIPAm [b]	Wt Fr NIPAm [c]	THF d*n*/dc [d] (mL/g)
$N_{52}D_{50}N_{41}$-C12	1	1.00	1.000	0.1310
	2	0.51	0.477	0.1747
	3	0.65	0.619	0.1628
$N_{35}D_{40}N_{42}D_{23}N_{22}$-C12	1	1.00	1.000	0.1310
	2	0.47	0.437	0.1780
	3	0.66	0.630	0.1620
	4	0.55	0.517	0.1714
	5	0.61	0.578	0.1663
C12-$N_{69}D_{60}N_{69}$-C12	1	1.00	1.000	0.1310
	2	0.70	0.671	0.1483
C12-$N_{46}D_{29}N_{46}D_{29}N_{46}$-C12	1	1.00	1.000	0.1310
	2	0.44	0.408	0.1706
	3	0.70	0.671	0.1483

[a] Nomenclature for triblocks (NDN) and pentablocks (NDNDN) of NIPAm (N) and DMA (D); the subscripted numbers denote the degree of polymerization of each corresponding block, based on ^{1}H NMR spectroscopy and assuming one RAFT agent per chain. The C12 represents the R-$C_{12}H_{25}$ chain end depending on the selected RAFT chain transfer agent. [b] Mole fraction of NIPAm, as determined by ^{1}H NMR spectroscopy. [c] Weight fraction of NIPAm, as determined by ^{1}H NMR spectroscopy. [d] Calculated using the homopolymer d*n*/dc values in this mobile phase.

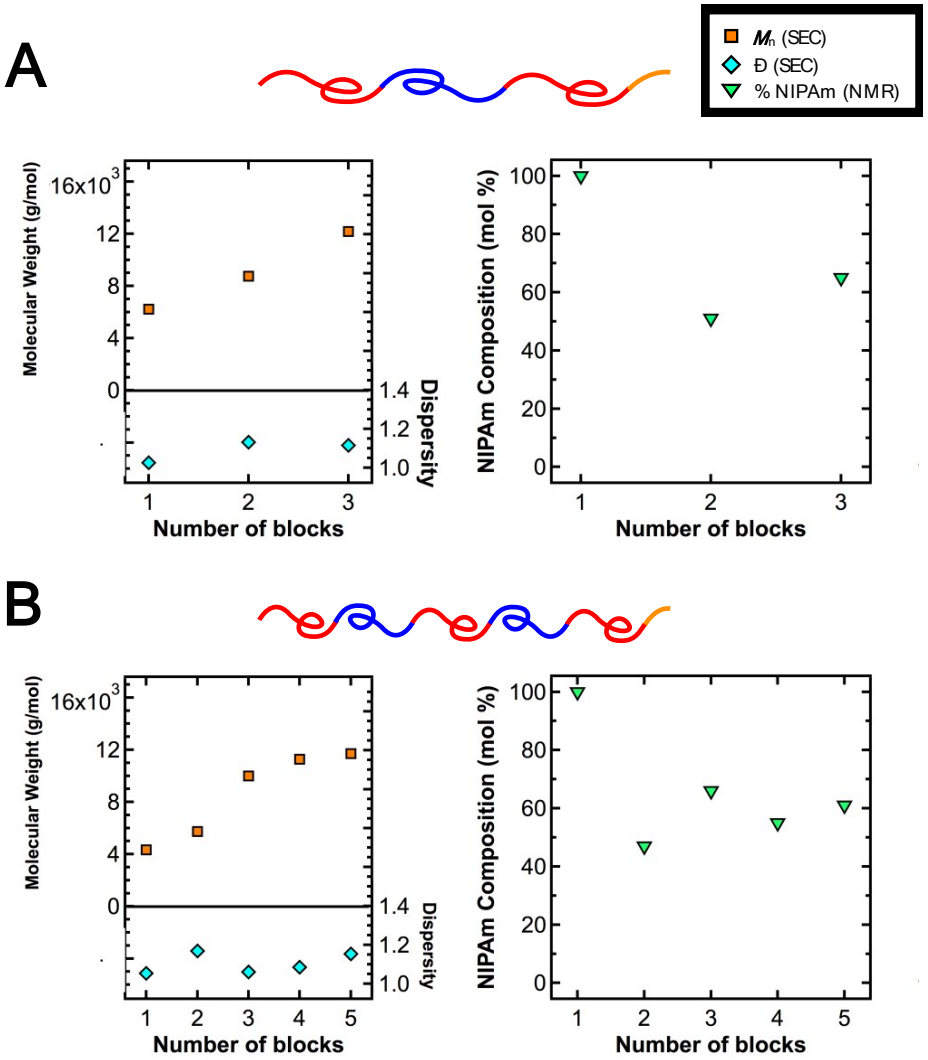

Figure S6. Molecular characterization of (A) $N_{52}D_{50}N_{41}$-C12 and (B) $N_{35}D_{40}N_{42}D_{23}N_{22}$-C12. The plots on the left show the evolution of the absolute number-average molecular weight (g/mol, measured by SEC-MALS) and dispersity with an increasing number of blocks. The plots on the right depict the evolution of the chemical composition (mol %, measured by ^{1}H NMR) of NIPAm with an increasing number of blocks.

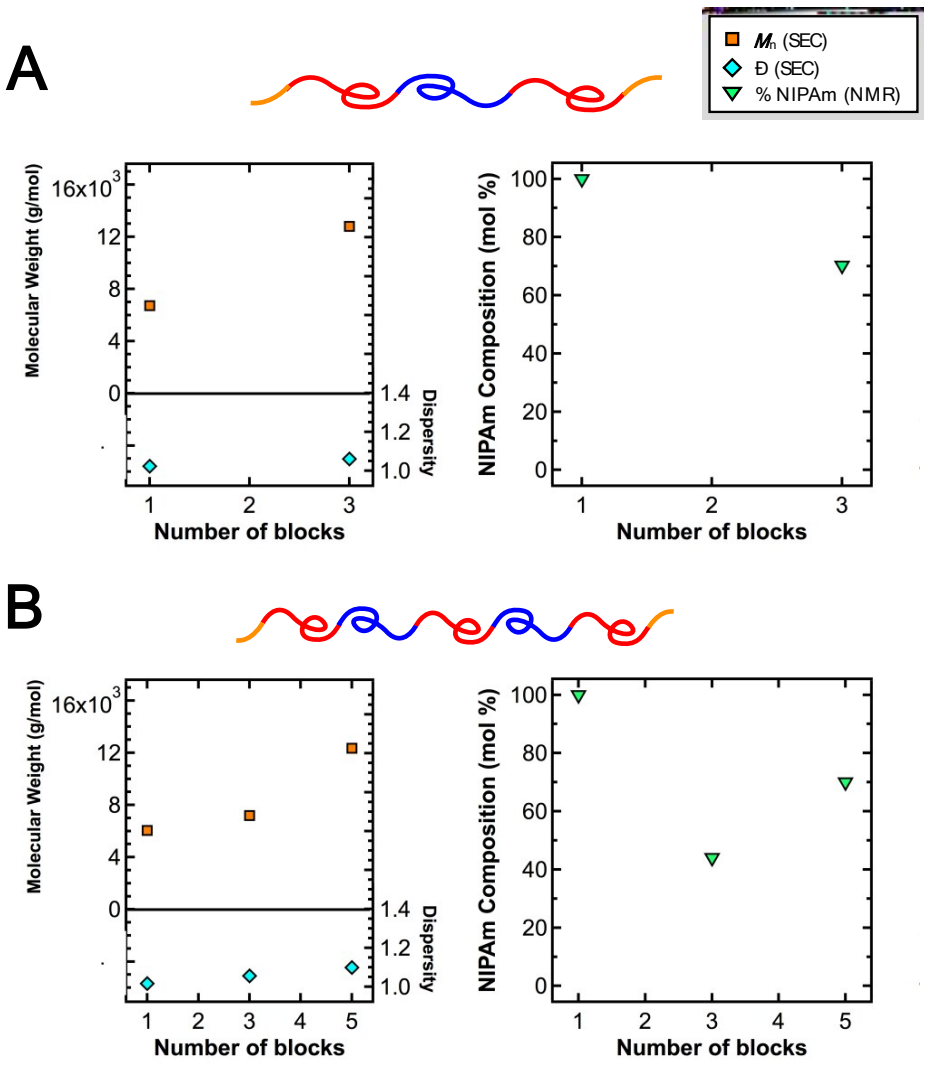

Figure S7. Molecular characterization of (A) C12-$N_{69}D_{60}N_{69}$-C12 and (B) C12-$N_{46}D_{29}N_{46}D_{29}N_{46}$-C12. The plots on the left show the evolution of the absolute number-average molecular weight (g/mol, measured by SEC-MALS) and dispersity with an increasing number of blocks. The plots on the right depict the evolution of the chemical composition (mol %, measured by ^{1}H NMR) of NIPAm with an increasing number of blocks.

2.4 End-group Removal Reactions and Characterization

The labile dodecyl thiocarbonylthio group was removed on select multiblock polymers for comparing solution-state behavior. This was accomplished using sequential aminolysis and

Michael addition reactions, following the work of Zhou *et al.*[7] A representative schematic of this reaction is shown in Scheme S1:

Scheme S1. Representative end-group removal reaction of C12-$N_{69}D_{60}N_{69}$-C12 triblock.

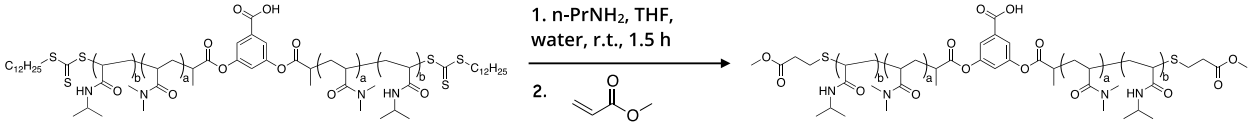

As seen in Fig. S8, the disappearance of the polymer trithiocarbonate peak at 310 nm in THF by UV-vis spectroscopy confirmed successful end-group removal for both polymer systems.

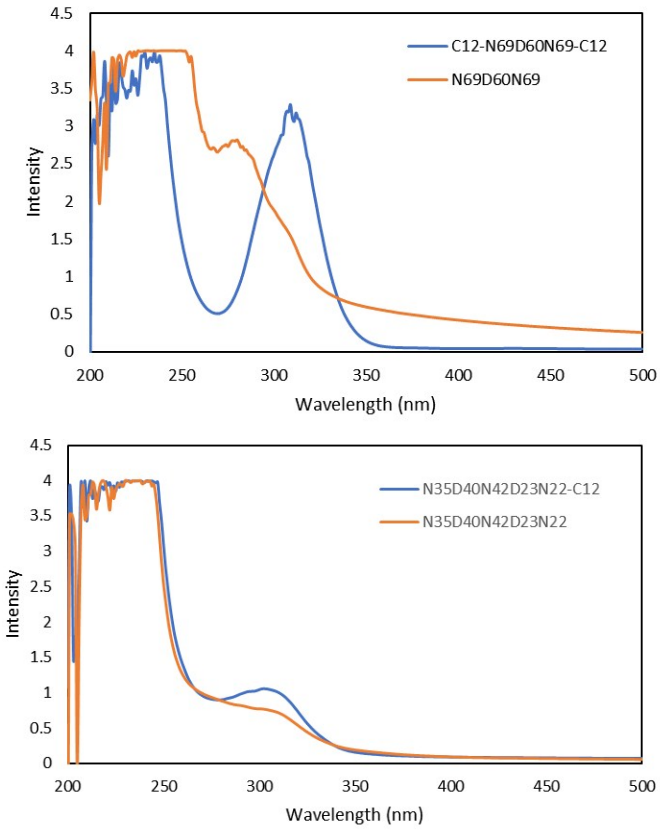

Figure S8. Representative UV-vis spectroscopy of C12-$N_{69}D_{60}N_{69}$-C12 triblock (top) and $N_{35}D_{40}N_{42}D_{23}N_{22}$-C12 pentablock (bottom) in THF before (blue) and after (orange) end-group removal.

3 Experimental: Thermoresponsive Characterization

3.1 Cloud Point Photos and Videos

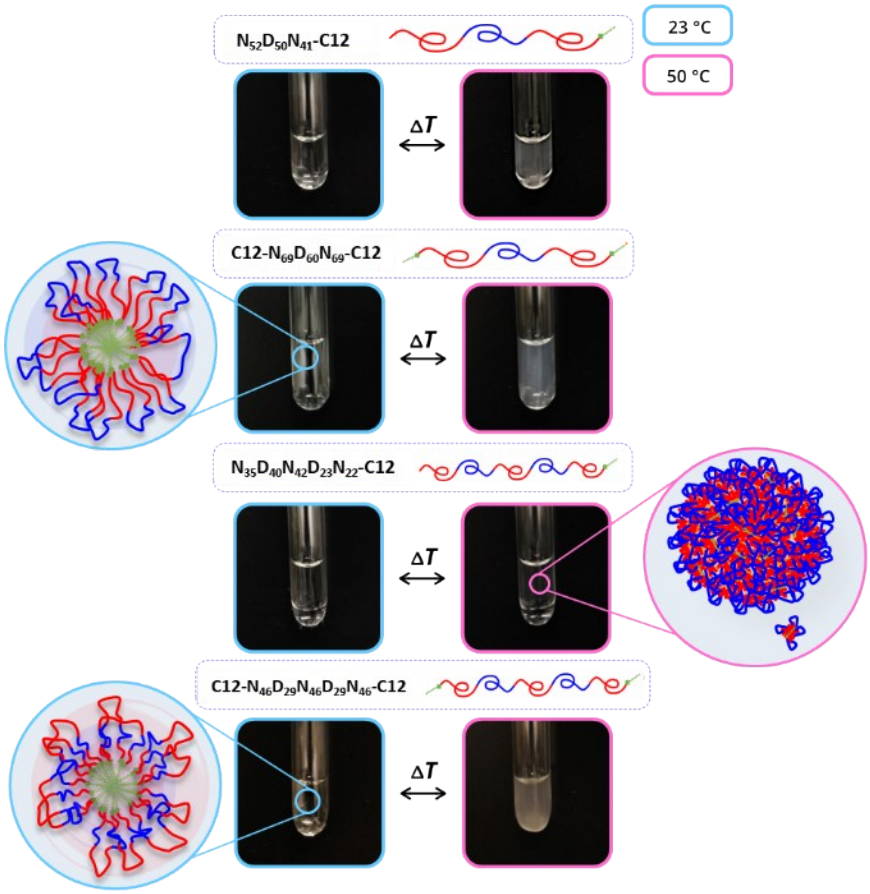

Figure S9. Photos of multiblock copolymers at room temperature and directly after heating to 50 °C.

Figure S10. Link to videos of solution thermoresponse upon heating for 1 mg/mL solution in PBS buffer.

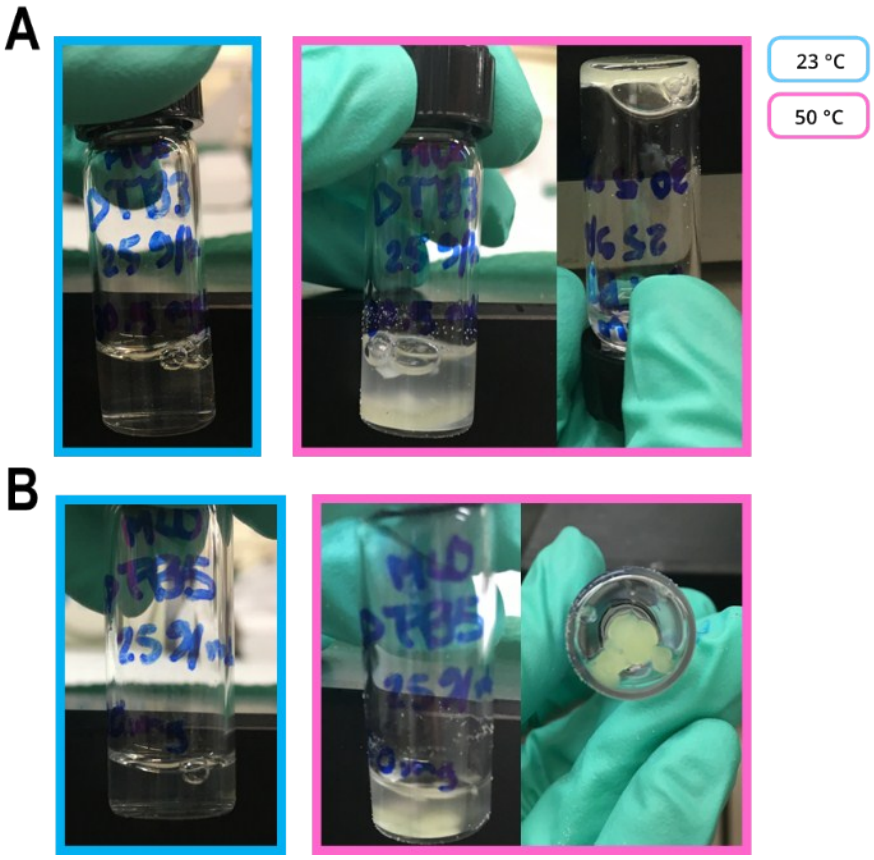

Figure S11. Photos of multiblock copolymers (A) C12-$N_{69}D_{60}N_{69}$-C12 and (B) C12-$N_{46}D_{29}N_{46}D_{29}N_{46}$-C12 at 25 mg/mL in solution upon heating to 50 °C and holding the sample at temperature for 10 min.

3.2 Detailed Cloud Point Temperature Characterization

For the systems that underwent end-group removal reactions, cloud point experiments were performed to examine the effects of the C12 tail(s). Fig. S12 and S13 show the heating and cooling profiles for the $N_{35}D_{40}N_{42}D_{23}N_{22}$-C12 (Fig. S12-A) and $N_{35}D_{40}N_{42}D_{23}N_{22}$ (Fig. S12-B)

pentablocks and the C12-$N_{69}D_{60}N_{69}$-C12 (Fig. S13-A) and $N_{69}D_{60}N_{69}$ (Fig. S13-B) triblocks, at 1 mg/mL, heated at rate of 0.25 °C/min and cooled under ambient conditions.

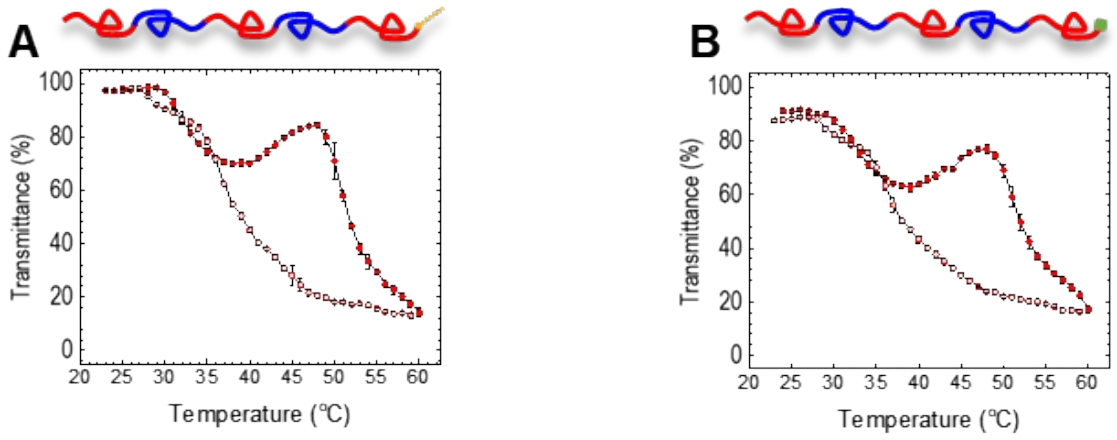

Figure S12. Cloud point curves upon heating (filled, red circles) and cooling (open, red circles) of investigated pentablocks (A) $N_{35}D_{40}N_{42}D_{23}N_{22}$-C12 and (B) $N_{35}D_{40}N_{42}D_{23}N_{22}$. Samples were heated at a rate of 0.25 °C/min and cooled under ambient conditions. The cloud point was defined as the temperature when the solution transmittance decreased to less than 80% of the value for the fully dissolved solution. Data points and vertical error bars denote the average and standard deviation, respectively, of over N = 30 measurements at each temperature.

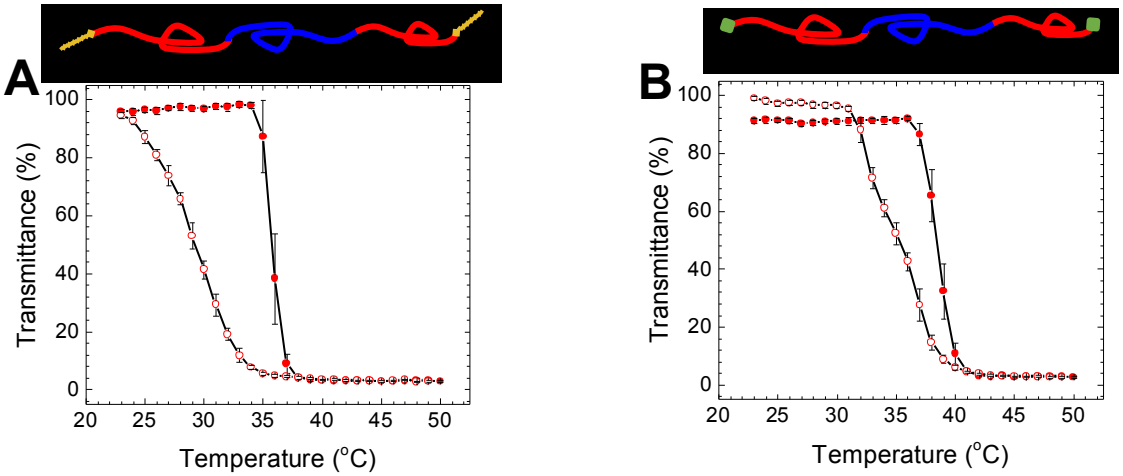

Figure S13. Cloud point curves upon heating (filled, red circles) and cooling (open, red circles) of investigated triblocks (A) C12-$N_{69}D_{60}N_{69}$-C12 and (B) $N_{69}D_{60}N_{69}$. Samples were heated at a rate of 0.25 °C/min and cooled under ambient conditions. The cloud point was defined as the temperature when the solution transmittance decreased to less than 80% of the value for the fully dissolved solution. Data points and vertical error bars denote the average and standard deviation, respectively, of over N = 30 measurements at each temperature.

4 Experimental: Solution Characterization

4.1 Static Light Scattering Experiments

Static light scattering (SLS) experiments were performed to estimate the micellar weight-average molecular weight (M_w) for the multiblock systems. Fig. S14 shows the partial Zimm analysis of C12-$N_{69}D_{60}N_{69}$-C12, C12-$N_{46}D_{29}N_{46}D_{29}N_{46}$-C12, and $N_{35}D_{40}N_{42}D_{23}N_{22}$-C12.

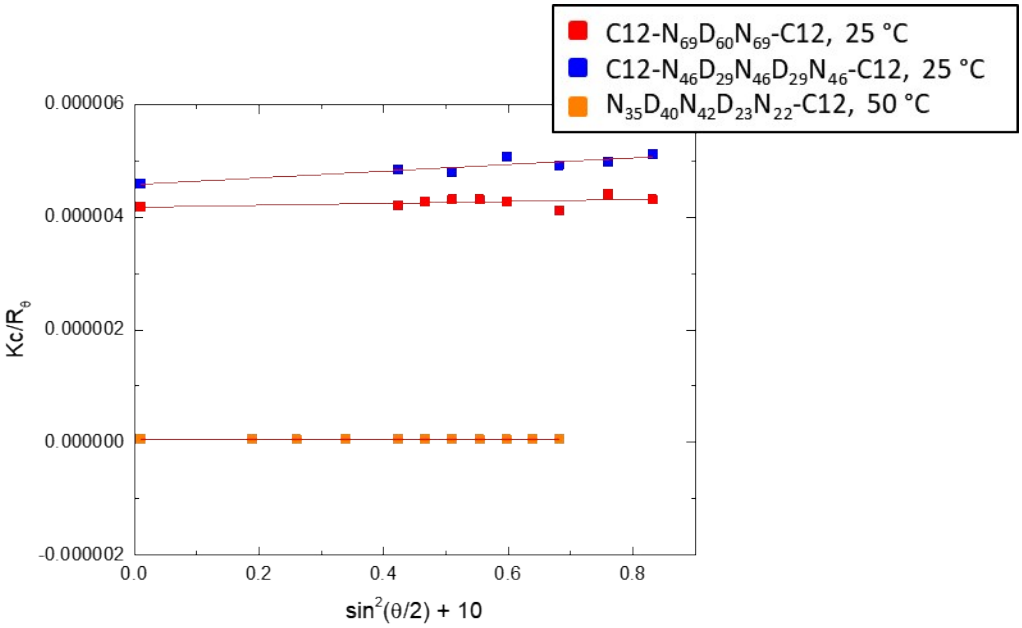

Figure S14. Partial Zimm analysis of C12-$N_{69}D_{60}N_{69}$-C12 (red squares), C12-$N_{46}D_{29}N_{46}D_{29}N_{46}$-C12 (blue squares), and $N_{35}D_{40}N_{42}D_{23}N_{22}$-C12 (orange squares) using SLS at 1 mg/mL. The red line shows the extrapolation to θ = 0.

The R_g of each structure was estimated using the slope of the Zimm approximation line using the following adaptation of the Zimm equation.

$$R_g^2 = \frac{3\lambda_0^2 M_w(slope)}{16\pi^2 n^2} \quad \text{(S-4)}$$

The calculated R_g for the C12-$N_{69}D_{60}N_{69}$-C12 and C12-$N_{46}D_{29}N_{46}D_{29}N_{46}$-C12 at 25°C were 13 and 23 nm, respectively. The calculated R_g for the $N_{35}D_{40}N_{42}D_{23}N_{22}$-C12 sample at 50°C was 32 nm.

Aggregate Structure Parameter and Density Calculations

The structure parameter, ρ, was calculated by taking the ratio of R_g/R_h and the aggregate density was calculated using the following equation:

$$\rho_{aggregate} = \frac{N_{agg} M_n}{N_{av}\left(\frac{4}{3}\pi R_h^3\right)} \quad \text{(S-5)}$$

The aggregate density of the C12-$N_{69}D_{60}N_{69}$-C12 and C12-$N_{46}D_{29}N_{46}D_{29}N_{46}$-C12 at 25°C was 0.09 and 0.08 g/mL, respectively. The structure parameters for the same samples were 1.3 and 2.2, respectively. The $N_{35}D_{40}N_{42}D_{23}N_{22}$-C12 sample at 50°C was calculated to be a less dense but still spherical particle with a density of 0.04 g/mL and structure factor of 0.54.

4.2 SAXS and Cryo-TEM Experiments

Small-angle X-ray scattering (SAXS) experiments were also conducted to probe the solution conformation at temperature settings below and above the cloud point. Fig. S15 shows

the collected SAXS patterns of the background PBS solution. We performed experiments with each polymer at 1 mg/mL in PBS solution. Unfortunately, subtracting the background from the data sets resulted in noise, indicating that the electron density difference between the NIPAm/DMA polymers was insufficient for SAXS detection.

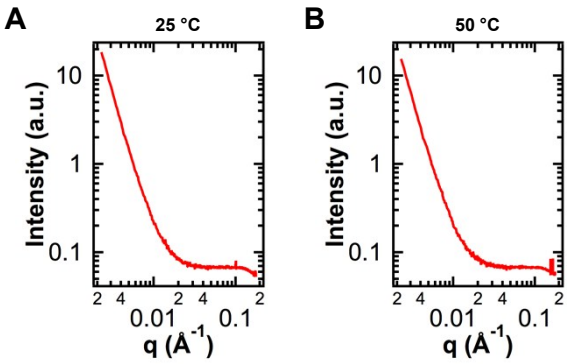

Figure S15. SAXS patterns of background phosphate buffer saline (PBS) solutions. SAXS experiments of PBS samples were conducted at (A) 23 °C and (B) 50 °C.

Finally, cryogenic-transmission electron microscopy (cryo-TEM) was employed to visualize these nanostructures in solution. At 23 °C, no structures could be visually detected. Fig. S16 shows select cryo-TEM images of the $N_{35}D_{40}N_{42}D_{23}N_{22}$-C12 at 1 mg/mL in PBS solution, vitrified from 50 °C in the preparation chamber. The average radius of 60 sphere-like particles was ~ 9.0 ± 2.1 nm. These measurements are about a sixth of the overall hydrodynamic size by DLS. Thus far, the structures of these pentablocks remain unclear, and future investigation is warranted.

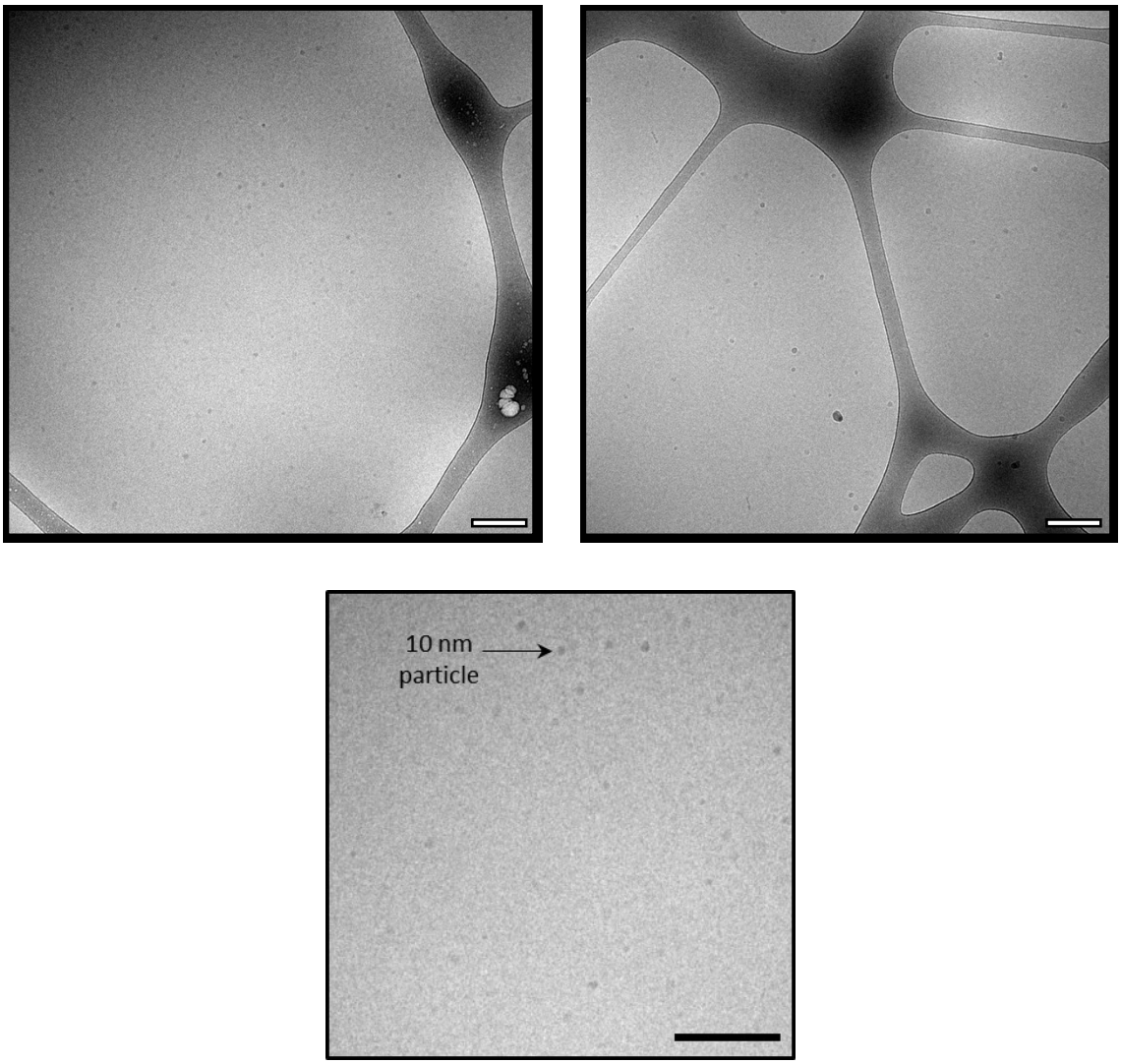

Figure S16. Cryo-TEM imaging of $N_{35}D_{40}N_{42}D_{23}N_{22}$-C12 micelles at 1 mg/mL in PBS solution, vitrified at 50 °C. Two representative images containing potential micelle-like structures are shown. The scale bars represent 200 nm. Cryo-TEM images taken by Yaming Jiang.

4.3 Diffusion-Ordered NMR Spectroscopy

The DOSY-NMR experiment premise is shown in Fig. S17. Consecutive gradient pulses with increasing magnetic field gradient strength attenuate ^{1}H NMR signals over time. The first encoding gradient pulse labels the initial locations of constitutive molecules; after a set period of time, a second decoding gradient pulse pinpoints the new locations of the molecules. Thus, from

the normalized relative intensities ($I/I(0)$) shown in Equation S-6, the translational diffusion coefficient (D_t) of the NIPAm and DMA chemical groups under the prepared solution conditions can be measured, given a specified gyromagnetic ratio of the observed nucleus (γ), gradient pulse (G_z), diffusion time (Δ), gradient length (δ):

$$I = I(0)e^{[-D_t\sqrt{(2\pi\gamma G_z)}((\Delta-\delta)/3)x10^4]} \quad \text{(S-6)}$$

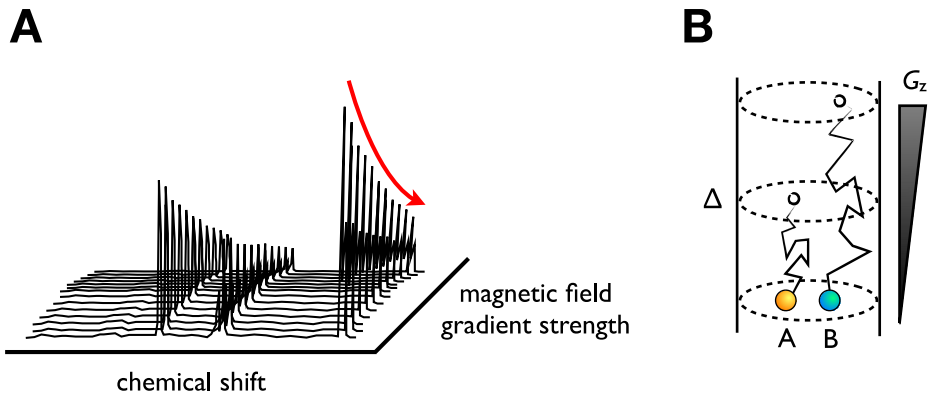

Figure S17. Schematic representation of diffusion-ordered NMR spectroscopy (DOSY-NMR) experiment. (A) Proton pulsed field gradients are sampled over increasing magnetic field gradient strength over time. The red arrow guides the decay of the signal intensity of a peak of interest. (B) The encoding gradient pulse G_z initially labels the spatial location of molecules A and B; after a specified diffusion time Δ, a second decoding gradient pulse identifies the translational movements of molecules A and B.

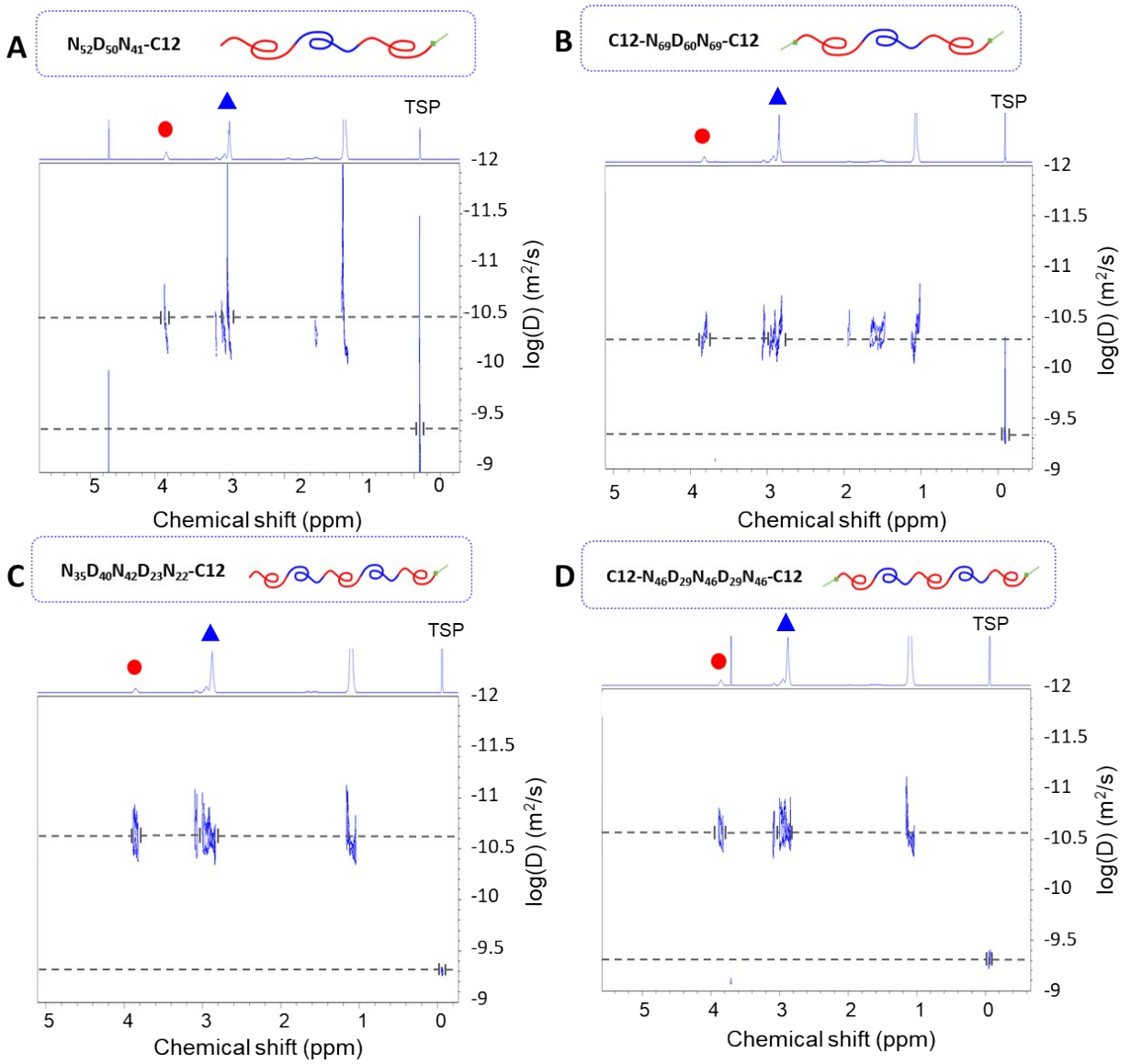

Figure S18. DOSY-NMR 2D spectra for the (A) $N_{52}D_{50}N_{41}$-C12, (B) C12-$N_{69}D_{60}N_{69}$-C12, (C) $N_{35}D_{40}N_{42}D_{23}N_{22}$-C12, and (D) C12-$N_{46}D_{29}N_{46}D_{29}N_{46}$-C12 multiblocks. The diffusion signal corresponds to the diffusion coefficient plotted on the y-axis of the two-dimensional plot. NIPAm (red circle) and DMA (blue triangle) signals correspond to the ^{1}H NMR peak at 4 and 2.8-3.3 ppm, respectively. TSP was used as a reference at 0 ppm.

Fig. S18 shows the ^{1}H NMR and diffusion profiles for each sample. Fig. S19 shows the fitted diffusion coefficient data for the prepared multiblock systems. The water-soluble internal standard trimethylsilyl propanoic acid (TSP) was used in all samples to ensure dilute solution conditions under the absence of viscous effects. There was close agreement between the ^{1}H signal

decays of NIPAm and DMA. Thus, for each sample the reported D_t values were averaged between the NIPAm and DMA D_t measurements. Table S2 summarizes the mean D_t values.

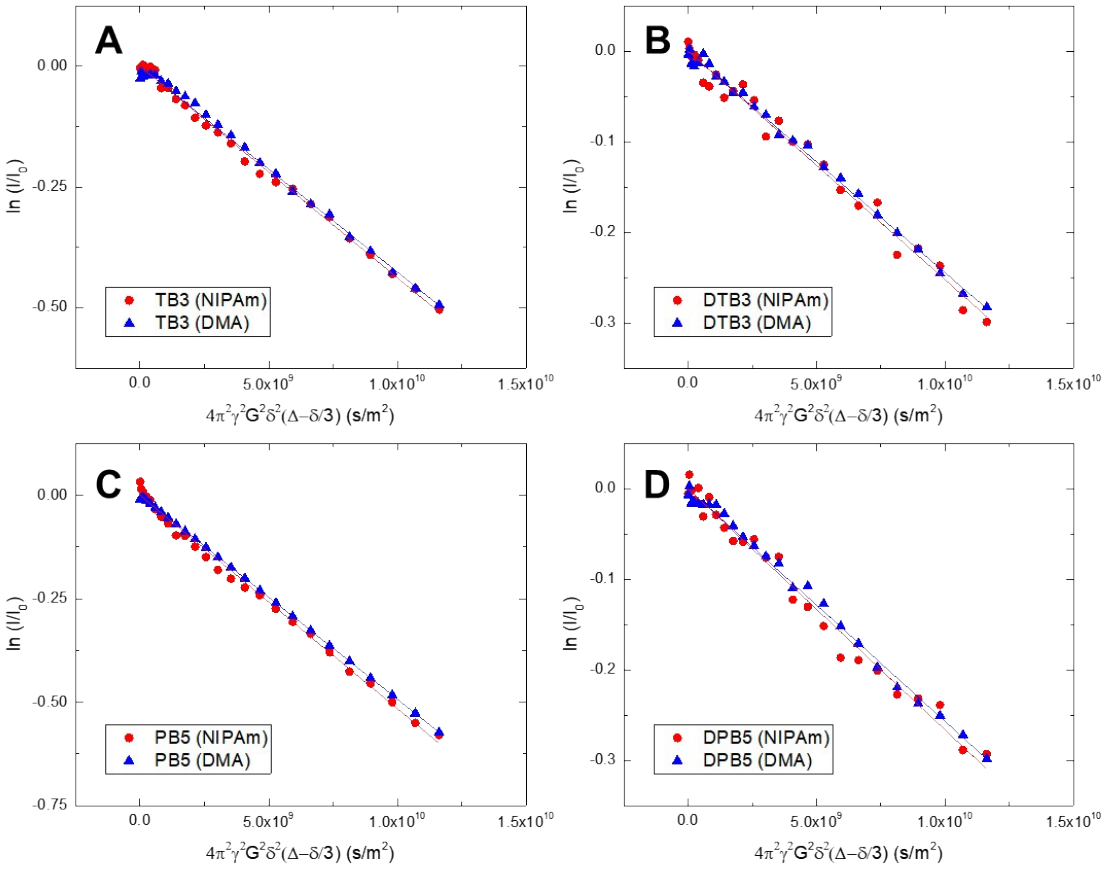

Figure S19. Representative diffusion coefficient fits from the proton signal intensity versus the variable pulse field gradient of (A) $N_{52}D_{50}N_{41}$-C12, (B) C12-$N_{69}D_{60}N_{69}$-C12, (C) $N_{35}D_{40}N_{42}D_{23}N_{22}$-C12, and (D) C12-$N_{46}D_{29}N_{46}D_{29}N_{46}$-C12 at 23 °C in D_2O. Both of the ^1H signal decays of NIPAm (red circles) and DMA (blue triangles) were plotted and fitted (red and blue lines, respectively).

Table S2. Summary of diffusion coefficients calculated by DOSY 2D NMR spectroscopy.*

System	$D \times 10^{-11}$, 27 °C (m²/s)			$D \times 10^{-11}$, 50 °C (m²/s)		
	Polymer	$\sigma_{polymer}$	TSP	Polymer	$\sigma_{polymer}$	TSP
$N_{52}D_{50}N_{41}$-C12	4.32	0.08	45.4	-	-	-
$N_{35}D_{40}N_{42}D_{23}N_{22}$-C12	5.00	0.14	44.9	89.6	7.3	909
C12-$N_{69}D_{60}N_{69}$-C12	2.47	0.03	49.0	-	-	-
C12-$N_{46}D_{29}N_{46}D_{29}N_{46}$-C12	2.62	0.06	48.3	-	-	-

* The numbers in the columns represent the diffusion coefficient (D) times 10^{-11}, e.g., the $N_{55}D_{53}N_{43}$-C12 polymer is 4.32×10^{-11} m²/s at 27 °C.

Finally, using the Stokes-Einstein equation the hydrodynamic radius R_h can be calculated under dilute conditions (Equation S-7). Here, k_B is Boltzmann's constant, T is temperature, and η is the dynamic viscosity.

$$D_t = \frac{k_B T}{6\pi R_h \eta} \tag{S-7}$$

4.4 Supplemental Dynamic Light Scattering Results

The following section shows the supplemental dynamic light scattering (DLS) details. Fig. S20 provides an overview of the autocorrelation functions fit with a second cumulant fit for the 90°-angle DLS data, collected at 25 °C and 1 mg/mL. More mathematical details for the cumulant fitting method are available elsewhere.[8] From this fitting, the decay rate (Γ, or inverse characteristic relaxation time) and magnitude of wavevector (q) were used with the Stokes-Einstein equation (Equation S-4a) to calculate the R_h and second-order polydispersity index (μ_2/Γ^2) of the sample population.

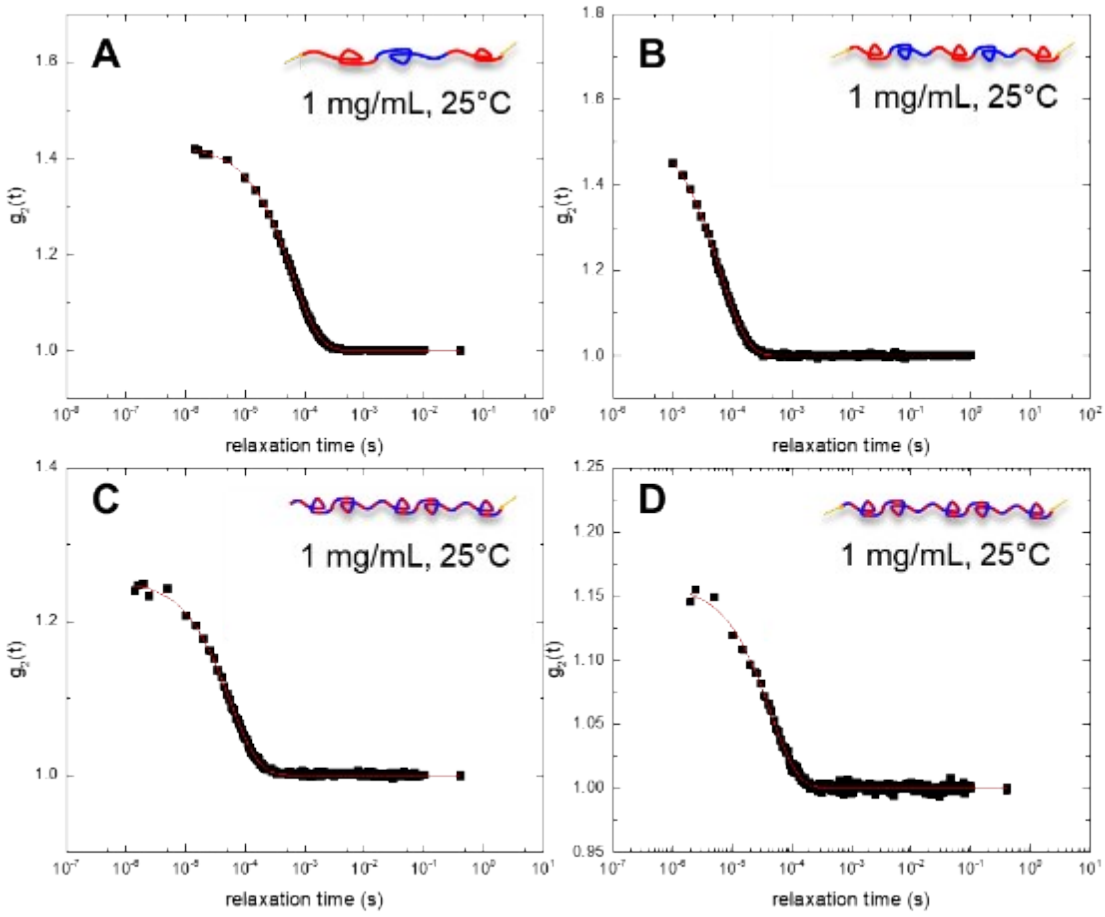

Figure S20. Representative autocorrelation functions fit (red curves) with a second cumulant fit for the 90°-angle DLS data (black squares) collected at 25 °C and 1 mg/mL; each fit was used to determine Γ and μ_2 to calculate the R_h and polydispersity of the population: (A) C12-$N_{69}D_{60}N_{69}$-C12, Γ = 8192 s^{-1}, $\mu_2 = 7.8 \times 10^6$ (B) C12-$N_{46}D_{29}N_{46}D_{29}N_{46}$-C12, Γ = 8176 s^{-1}, $\mu_2 = 5.9 \times 10^6$ (C) poly(N-*co*-D)$_{107}$-C12, Γ = 9095 s^{-1}, $\mu_2 = 1.7 \times 10^7$ (D) C12-poly(N-*co*-D)$_{129}$-C12, Γ = 11,570 s^{-1}, $\mu_2 = 1.7 \times 10^7$.

In addition, Figs. S21 and S22 show representative cumulant fittings for the $N_{35}D_{40}N_{42}D_{23}N_{22}$-C12 and C12-$N_{46}D_{29}N_{46}D_{29}N_{46}$-C12 pentablocks across multiple scattering angles. The Γ versus q^2 plots are linearly related and closely intersect the origin at $q = 0$, verifying the diffusive nature of the particles and the appropriateness of employing the Stokes-Einstein equation.

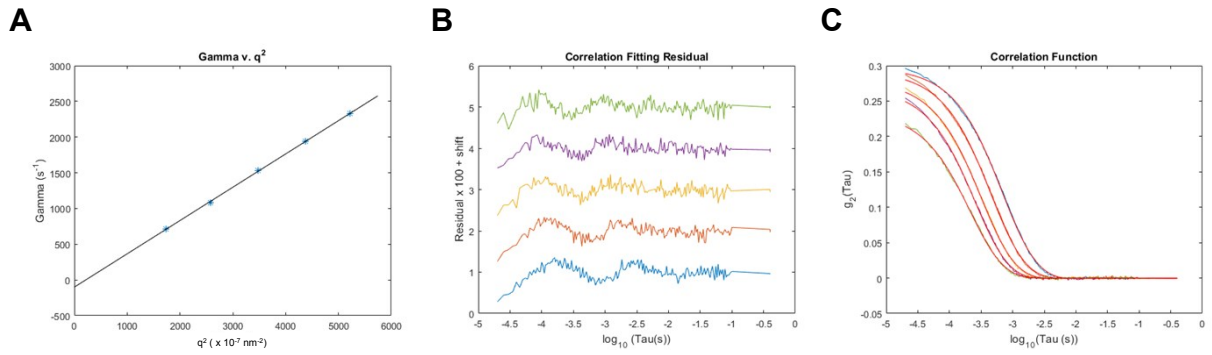

Figure S21. Detailed DLS analysis using a cumulant fit of $N_{35}D_{40}N_{42}D_{23}N_{22}$-C12 pentablock at 1 mg/mL in PBS solution at 23 °C: (A) gamma (decay rate) versus q^2 plot, (B) correlation fitting residuals, and (C) autocorrelation function fittings. DLS measurements were collected from 60 to 120° in 15° increments.

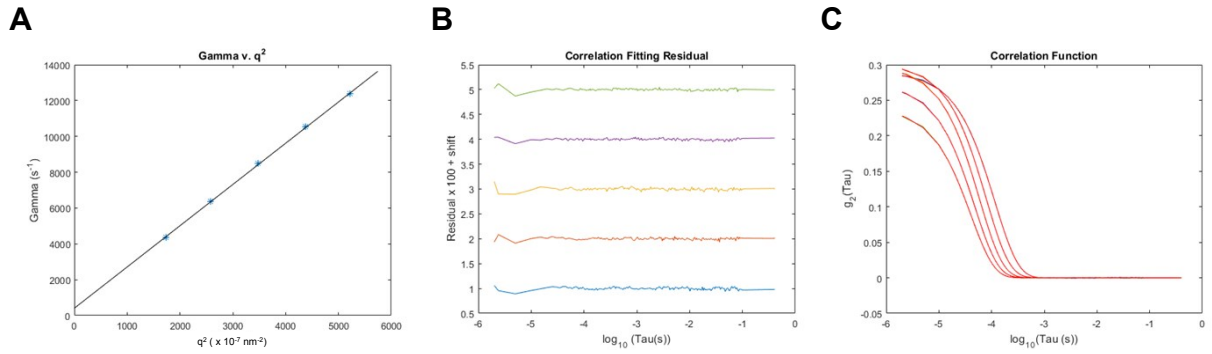

Figure S22. Detailed DLS analysis using a cumulant fit of C12-$N_{46}D_{29}N_{46}D_{29}N_{46}$-C12 pentablock at 1 mg/mL in PBS solution at 23 °C: (A) gamma (decay rate) versus q^2 plot, (B) correlation fitting residuals, and (C) autocorrelation function fittings. DLS measurements were collected from 60 to 120° in 15° increments.

Fig. S23 shows the hydrodynamic radius distribution changes for $N_{52}D_{50}N_{41}$-C12, C12-$N_{69}D_{60}N_{69}$-C12, and C12-$N_{46}D_{29}N_{46}D_{29}N_{46}$-C12 with increasing temperature. As the sample approaches its T_{CP}, the distribution first sharpens due to the PNIPAm coil-to-globule collapse before large

aggregate populations appear indicative of phase separation and the sample becoming turbid as shown in Fig. S9.

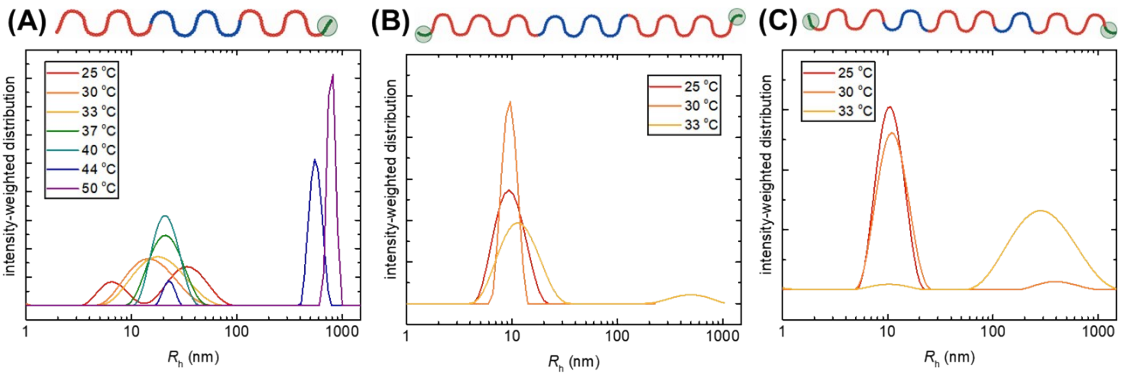

Figure S23. Variable-temperature DLS measurements for (A) $N_{52}D_{50}N_{41}$-C12, (B) C12-$N_{69}D_{60}N_{69}$-C12, and (C) C12-$N_{46}D_{29}N_{46}D_{29}N_{46}$-C12.

Finally, Fig. S24 shows the supporting DLS data for the $N_{35}D_{40}N_{42}D_{23}N_{22}$-C12 pentablock for end-group comparison at 50 °C. The -$C_{12}H_{25}$ end group was removed according to the reaction shown in Scheme S-1. Fig. S25 shows the hydrodynamic radius distribution of C12-$N_{69}D_{60}N_{69}$-C12 and $N_{69}D_{60}N_{69}$ triblocks at 1 and 10 mg/mL concentrations.

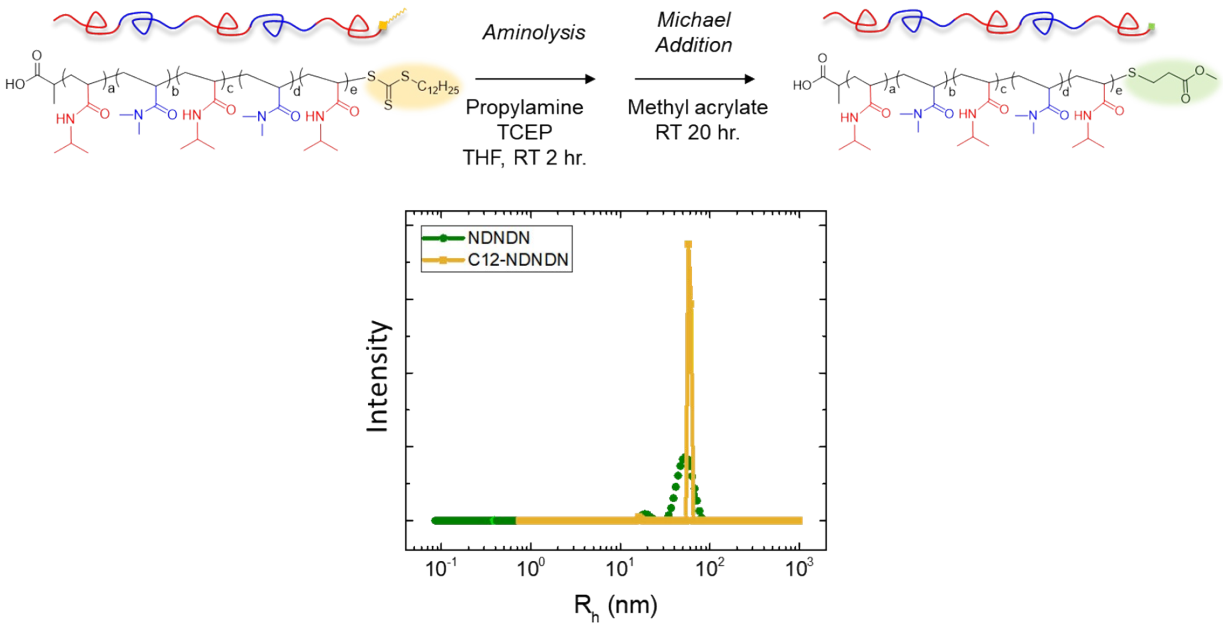

Figure S24. Hydrodynamic radius distribution obtained via a REPES Laplace inversion from DLS data for $N_{38}D_{43}N_{46}D_{25}N_{23}$-C12 (gold curve) and $N_{38}D_{43}N_{46}D_{25}N_{23}$ (green curve) at 1 mg/mL in PBS buffer at 50 °C at an angle of 90°.

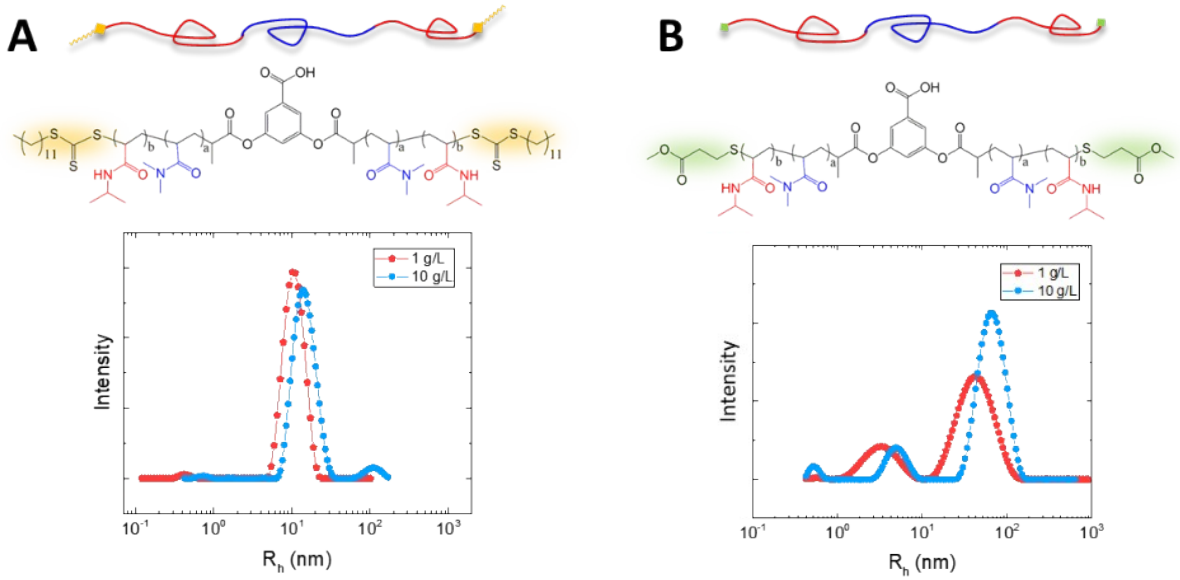

Figure S25. Hydrodynamic radius distribution obtained via a REPES Laplace inversion from DLS data for triblocks (A) C12-$N_{69}D_{60}N_{69}$-C12 and (B) $N_{69}D_{60}N_{69}$ at 1 and 10 mg/mL in PBS buffer at 25 °C.

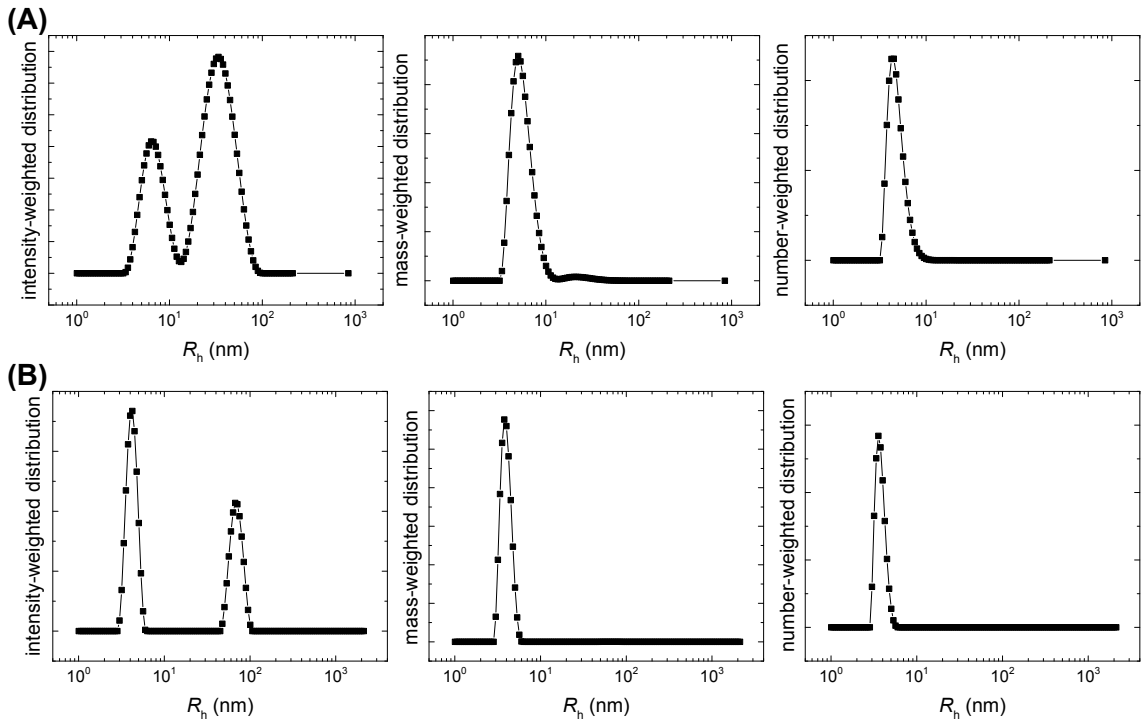

Figure S26. The R_h distribution for (A) $N_{52}D_{50}N_{41}$-C12 and (B) $N_{35}D_{40}N_{42}D_{23}N_{22}$-C12 in terms of intensity-weighted, mass-weighted, and number-weighted distributions (from left to right). The mass-weighted and number-average distributions were calculated assuming that intensity from light scattering scales as R_h^3 and R_h^6, respectively. The aggregated population in the triblock sample makes up less than 10% of the population by mass and less than 1% of the population by number. The pentablock copolymer aggregate represents less than 1% of the population by mass and number. Therefore, the majority population in each sample at 1 mg/mL in PBS buffer is free polymer chains.

5 Author Roles and Responsibilities

All authors have read and approved the completed manuscript. M.L.O. led the light scattering and DOSY NMR experiments, post-synthetic modification experiments, synthesis and characterization of statistical polymer samples, drafted the sections covering these topics, and was the major contributor in preparing the final manuscript. J.M.T. led the design of experiments, conducted general synthesis and characterization experiments, and drafted the preliminary manuscript. S.D.J. designed the experiments for the multiblock synthesis and characterization. S.J. provided assistance with light scattering analysis and interpretation. F.S.B. and T.M.R. were the co-principle investigators of the project and directed the research, managed the project, and contributed to the data analyses and interpretation of the experiments.

6 References

1 G. Moad, R. T. A. Mayadunne, E. Rizzardo, M. Skidmore and S. H. Thang, 2003, **2**, 520–535.

2 G. Gody, T. Maschmeyer, P. B. Zetterlund and S. Perrier, *Macromolecules*, 2014, **47**, 639–649.

3 J. Jakeš, *Collect. Czechoslov. Chem. Commun.*, 1995, **60**, 1781–1797.

4 J. M. Ting, S. Tale, A. A. Purchel, S. D. Jones, L. Widanapathirana, Z. P. Tolstyka, L. Guo, S. J. Guillaudeu, F. S. Bates and T. M. Reineke, *ACS Cent. Sci.*, 2016, **2**, 748–755.

5 U. Nobbmann, The Chromatogram Series: PNIPAm, https://www.materials-talks.com/blog/2014/01/16/the-chromatogram-series-pnipam/, (accessed 18 April 2018).

6 E. Read, A. Guinaudeau, D. J. Wilson, A. Cadix, F. Violleau and M. Destarac, *Polym. Chem.*, 2014, **5**, 2202–2207.

7 C. Zhou, M. A. Hillmyer and T. P. Lodge, *Macromolecules*, 2011, **44**, 1635–1641.

8 D. E. Koppel, *J. Chem. Phys.*, 1972, **57**, 4814–4820.